Research Article

Fabrication of CdS quantum dots sensitized TiO_2 nanowires/nanotubes arrays and their photoelectrochemical properties

Hua Lin[1] · Zhou Mao[1] · Ningjin Zhou[1] · Meng Wang[1] · Lu Li[1] · Qing Li[1]

Abstract

Herein, CdS quantum dots (QDs) sensitized TiO_2 nanowires/nanotubes arrays (CdS–TiO_2 NWs/NTs) have been successfully fabricated through an optimized one-step anodization method, followed by successively ion layer adsorption and reaction strategy. The structures of the as-prepared samples were characterized by scanning electrons microscopy, X-ray diffraction and X-ray photoelectron microscopy. Results indicated that TiO_2 NWs/NTs were comprised of well-ordered NTs arrays in the bottom and NWs at the mouth of the NTs. CdS QDs were uniformly adhered to the surface of the NWs, as well as inner walls of the NTs. In addition, optical and photoelectronchemical properties of the as-prepared samples were investigated. All results showed that CdS–TiO_2 NWs/NTs exhibited excellent photoelectric and photocatalytic activities, a photocurrent density of 1.04 mA cm^{-2}, a photocatalytic efficiency of degradation methyl blue of 97.8% after 120 min, and the rate of repeated degradation maintained at 95.8% after 5 cycles. A possible mechanism was described to lay the foundation for future applications.

Keywords TiO_2 NWs/NTs arrays · CdS · Photoelectric performance · Photocatalytic activity

1 Introduction

Over the past few decades, Titanium dioxide (TiO_2) has been received great attentions and considered as an ideal photocatalyst for solar cells and environmental purification due to its outstanding photoelectrochemical properties [1–4]. Compared with pulverous TiO_2, highly ordered nano-structures like nanowires (NWs), nanobelts (NBs), nanorods (NRs), nanoflakes (NFs) and nanotubes (TNs) have been as more effective architectures to improve the photocatalytic efficiency [5–8]. Among these, TiO_2 TNs have been regard as the most promising nanostructures for future application with remarkable light-harvesting properties, recyclability and high mass transport efficiency, in which photogenerated carriers can be easily transported along its ordered structures [9, 10].

Actually, enhancing its photocatalytic efficiency for future applications, it requires further enlarging the specific surface area to increase reactive sites and adsorption capacity of the reactants [11, 12]. Usually, the way of increasing the specific surface area is to extend the length of TiO_2 TNs, Nevertheless, which would increase the recombination of electron–hole pairs during long distance transmission. Therefore, the challenge of how to further improve the specific surface area of TiO_2 NTs with low recombination still remains. Moreover, TiO_2 is a wide band gap semiconductor, it can only be excited by UV light, hence, only 2–3% solar energy can be used. Thus, numerous attempts were carried out to narrow this band gap and improve the light absorption capacity in the visible region, such as using non-metallic element doping (N, C, S, I, F) [13–15], organic dyes or metal chalcogenide

Electronic supplementary material The online version of this article (https://doi.org/10.1007/s42452-019-0420-9) contains supplementary material, which is available to authorized users.

✉ Hua Lin, lh2004@swu.edu.cn | [1]School of Materials and Energy, Southwest University, No. 2 Tiansheng Road, Beibei District, Chongqing 400715, China.

SN Applied Sciences (2019) 1:391 | https://doi.org/10.1007/s42452-019-0420-9

Received: 9 November 2018 / Accepted: 27 March 2019 / Published online: 2 April 2019

quantum dots (QDs) sensitizing [16, 17], depositing noble metal nanoparticles (Au, Ag, Pt) [18–20], etc. Among these methods, QDs sensitized TiO_2 was considered the best strategies to improve spectral absorptivity and electron transfer ability, with a vast amount of studies being reported, these include CdSe, CdS, CdTe, PbS, ZnS, PbSe and InP [21–25]. In the case of CdS, which has a narrow band gap (2.2 eV), it is a promising material for decorating TiO_2, leading to a red shift of light absorption to visible light [26, 27]. By directly loading QDs onto the surface of TiO_2 NTs, however, an accumulation at the NTs mouth would occur, which consequently seriously affects the efficiency of photoelectric conversion.

To overcome these problems, this work discovered a facile and effective synthetic strategy for the fabrication of a novel composite structure of TiO_2 NWs/NTs with CdS QDs, resulting in excellent photocatalysis and photoelectronic properties. In TiO_2 NWs/NTs structures, highly ordered NTs arrays were prepared on a Ti film, NWs were generated through splitting of the top of the NTs, which meaned that the NWs and the NTs was an organic whole. This unique structure is not only beneficial to utilizing the advantages of TiO_2 NTs in efficiently transporting the photogenerated carriers, but also to increasing the specific surface area of TiO_2 for loading additional QDs. The SILAR method was then used to synthesize CdS QDs to adhere to the TiO_2 composite structure. The results showed that the compound possesses excellent photoelectrical performance and photocatalytic efficiency as well as high reusability rate.

2 Materials and methods

2.1 Experimental

The TiO_2 NWs/NTs arrays were fabricated using the anodic oxidation method. In a typical experiment, Tailored Ti foil (99.6% pure, 1 cm × 1 cm × 0.02 cm) was successively ultrasonic cleaned by acetone, isopropanol, ethanol and distilled water. Then the cleaned Ti foil was polished in a mixed solution of hydrofluoric acid and nitric acid for 30 s. The anodic oxidation process was conducted in ethylene glycol solution (include 0.3 wt% NH_4F and 2 vol% H_2O) by 55 V DC power for 5 h. The as-anodized Ti foil was cleaned by distilled water several times and then annealed in a muffle furnace at 500 °C in atmosphere for 3 h with a heating rate of 5 °C/min.

In SILAR process, the prepared TiO_2 NWs/NTs arrays were successively dipped into ethanol + 0.1 M $CdCl_2$ and methanol + 0.1 M Na_2S for 5 min each time, respectively. After one immersion procedure, the sample was washed with ethanol and methanol to remove excess reagent, and then dried before entering the next dipping cycle. After this process, the prepared sample was annealed at 350 °C for 1 h in vacuum to obtain a more stable heterojunction. The prepared samples were respectively called CTWT$_0$, CTWT$_1$, CTWT$_2$ and so on, according to the number of SILAR deposition cycles.

2.2 Characterizations

Crystal structure of the samples were characterized by X-ray diffraction (Shimadzu, XRD-6100) with Cu Kα irradiation (λ = 0.15418 nm) at a scanning rate of 4° min^{-1} in the range of 20° ≤ 2θ ≤ 80°. The surface morphology and the elemental concentration and distribution were analyzed by an energy dispersive spectrometer (EDS) attached to the field emission scanning electron microscopy (JSM-7800 FESEM). The chemical composition and electronic structure were determined through X-ray photoelectron spectroscopy (XPS, ESCALAB 250XI) using Al *Kα* (hv = 1486.6 eV) irradiation with the electron energy analyzer operating at constant transmission energy (30 eV) and the measurement was performed under ultrahigh vacuum conditions 10^{-10} Torr. The UV–Vis absorption spectra were measured by a UV–visible spectrophotometer (Hitachi, U-3310). Photoluminescence measurements were performed on a fluorescence spectrophotometer (Hitachi, F-7000) using Xe lamp as excitation source.

The photoelectric behaviors were characterized using CHI 760E electrochemical workstation, a 300 W Xe lamp was used as the simulated solar light source, 0.5 mol L^{-1} Na_2SO_4 solution was used as electrolyte, whereas Pt foil and saturated Ag/AgCl were used as counter and reference electrodes, respectively. The current–voltage characteristics was tested from open circuit voltage to 1 V at a scan rate of 0.05 V s^{-1}, and the transient current–time characteristics was measured at a bias voltage of 0.6 V for 380 s with an interval of 20 s between dark and light. To detect the photocatalytic efficiency of the prepared samples, 30 mL MB solution (5 mg L^{-1}) was used as the contaminant in the photocatalytic test process, and this process was conducted under the same Xe lamp light source at room temperature.

3 Results and discussion

3.1 Morphological and elemental analysis

Figure 1 shows the FESEM images of TiO_2 NWs/NTs arrays with different deposition times of CdS through SILAR method. As shown in Fig. 1a, the bare TiO_2 NWs/NTs is comprised of well-ordered NTs structures in the bottom with an average diameter of 80 nm, TiO_2 NTs wall thickness

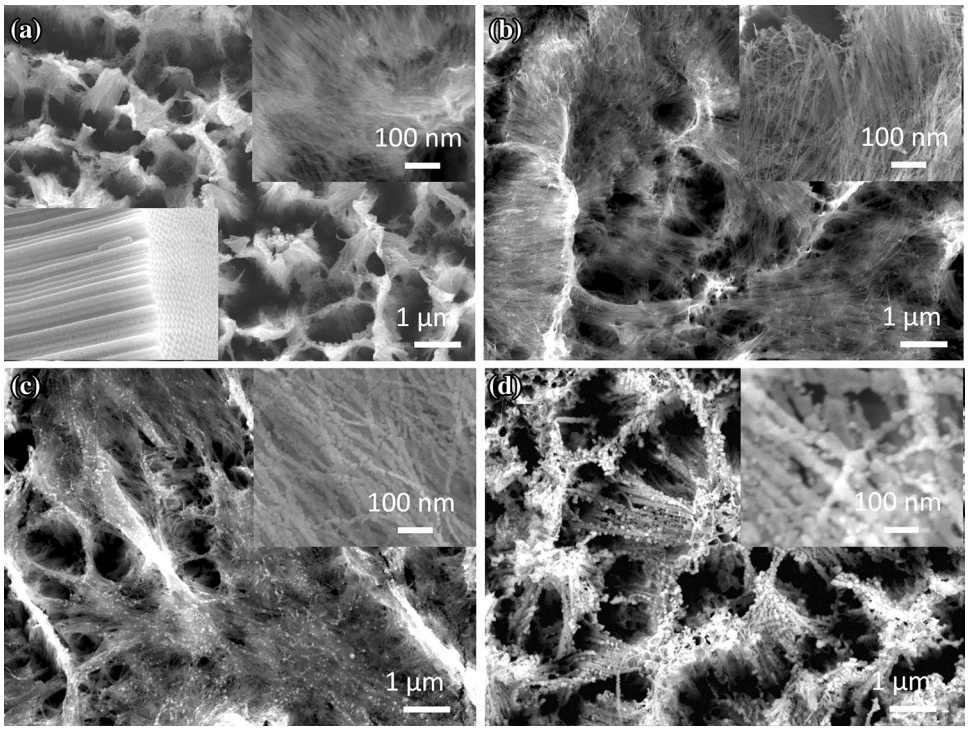

Fig. 1 FESEM images of different samples of CdS–TiO_2 NWs/NTs arrays: **a** $CTWT_0$; **b** $CTWT_1$; **c** $CTWT_3$; **d** $CTWT_5$; the insert is the top enlarged morphology of the as-prepared samples

is ca. 10 nm, and the orderly growth of NWs at the mouth of the NTs. NWs diameter is ca. 3–5 nm and ca. 1–2 μm in length, as shown in the insert image (the upper-left corner is the magnification of the top of NMs, the bottom-right is the magnification of the bottom of NTs). The anodic oxidation process can be believed that the TiO_2 NTs were firstly formed at the film of Ti foil, and then the mouth of NTs would be split into NWs with increasing electrolytic time, resulting a combined structure covered well-arranged NTs in the bottom and NWs in the top. Undoubtedly, the electrolytic voltage and electrolysis time is the key to generating a good NWs/NTs structure. Many reports have indicated that only TiO_2 NTs can be obtained at 20–30 V electrolytic voltage [28, 29]. Similarly, experiments have shown that NTs were obtained within 3 h of electrolysis, in which all wires were without any NTs after electrolysis for 7 h owing to the excessive anodic oxidation time (show in Fig. S1). Herein, the anodic oxidation condition was controlled at 55 V for 5 h. Compared with other reports, our approach can simplify the operation process (one-step composition) and greatly shorten the reaction time [30]. Figure 1b shows the top view of $CTWT_1$, only a small amount of QDs was deposited on TiO_2 NWs/NTs arrays due to the SILAR cycle time being too small. By increasing the number of SLAR cycles, the quantity of CdS QDs expanded greatly, as shown in Fig. 1c. From the insert diagram, it can be seen that CdS QDs were displayed a spherical structures particle with an average diameter of 6–8 nm and uniformly adhered on the surface of NWs. However, with an increase in the number of cycles, QDs aggregation easily occurred on the surface of NWs/NTs, as shown in Fig. 1d, the surface of NWs were covered with a thick layer of QDs. The results indicate that the SILAR is an effective way of depositing CdS QDs on TiO_2 NWs/NTs, with the QDs uniformly adhering to the NWs and inner wall of NTs. When compared to the NTs structure, this unique structure can provide greater surface area for more QDs deposited on their face, which can enhance photon absorption ability and improve photoresponse efficiency.

The crystal structures of the as-prepared samples were characterized and the XRD results were shown in Fig. 2a. In the case of bare TiO_2 NWs/NTs arrays (Fig. 2a(1)), all diffraction peaks are attributed to anatase TiO_2 (JCPDS No.89-4921) and Ti substrates (JCPDS No. 89-5009), respectively. As shown on the Fig. 2a(2–4), the weak diffraction peaks at 26.5°, 43.9°, 52.1° correspond to the (111), (220), (311) crystal plane of CdS QDs (JCPDS No. 75-1546), the other CdS diffraction peaks were not identified due to overlapping with anatase TiO_2 and Ti substrate peaks [1]. The XRD patterns indicated that these composite materials consist of CdS, TiO_2 and Ti, which showed that CdS QDs were successfully deposited on the TiO_2 NWs/NTs arrays. The EDS spectra of the sample $CTWT_3$ displays the distribution of the atomic and weight composition, as shown in Fig. 2b, and the presence of Ti, O, Cd, S, C elements, which is consistent with the XRD and FESEM results. Furthermore, the ratio of atomic composition of Cd:S is close to 1:1, demonstrating that the

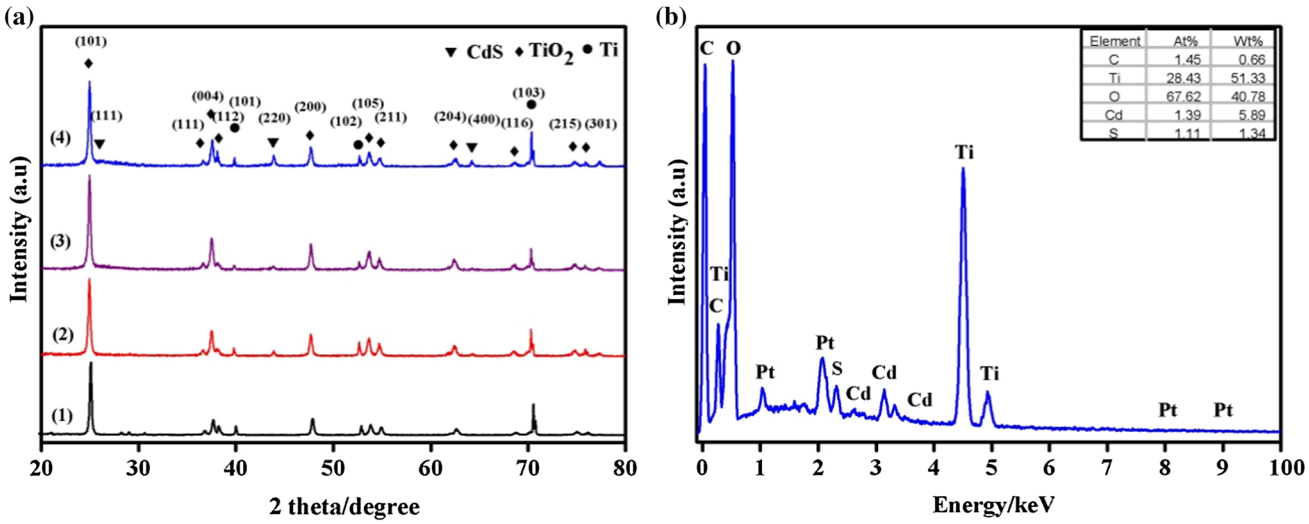

Fig. 2 **a** XRD patterns of different samples of CdS–TiO_2 NWs/NTs arrays: (1) $CTWT_0$; (2) $CTWT_1$; (3) $CTWT_3$; (4) $CTWT_5$; **b** EDS spectrum of the sample $CTWT_3$

prepared QDs are without other impurities, and that the ratio of Ti:O is more than 1:2 attributing to the surplus O absorbed by the sample. In addition, there is an intense peak from C element, which may be the consequence of C absorption from the air or the stained ethylene glycol be carbonized during the annealing process [31].

To conduct a detail investigation of the chemical components and electronic structure of the $CTWT_3$ sample, XPS analytical technique was performed. The analysis of XPS spectra was preceded using XPSPEAK 4.1 software and the peak positions of core level spectra were calibrated with C 1s at 284.6 eV [32]. Survey spectra of the sample was shown in Fig. 3a, where all of core level spectra of the element such as Ti, O, Cd, C and S were existed without impurity. From the insert table, it can be seen that atomic ratio of sulfur to cadmium is about 1:1, and carbon and excess oxygen may be due to the contamination of the sample exposed to the air. As shown in Fig. 3b, the binding energy of Cd 3d is located at 405.7 and 412.4 eV individually, due to Cd $3d_{5/2}$ and Cd $3d_{3/2}$ of CdS QDs. The binding energy of S 2p is at 161.8 and 168.8 eV (Fig. 3c), which demonstrates the presence of the S element in the samples, with S^{2-} valence state. From Fig. 3d, the energy located at 459.0 and 464.8 eV corresponds to Ti $2p_{3/2}$ and Ti $2p_{1/2}$. Additionally, O1s is observed at 528.2–535.3 eV, the peaks at 530.22 and 531.8 eV can be assigned to the O–Ti–O bond and hydroxyl oxygen (OH^-), respectively, which mainly originate from air. The results were consistent with the EDS patterns, which further confirmed that CdS QDs have been successfully deposited on TiO_2 NWs/NTs arrays.

3.2 Optical and photoelectrical properties

The UV–Vis absorption spectra of the $CTWT_0$ and $CTWT_3$ samples are shown in Fig. 4a with a wavelength range 300–760 nm. We observed that the bare TiO_2 NWs/NTs arrays could only absorb UV light below 380 nm, when those sensitized using CdS QDs (Fig. 4a(2)) were examined the absorption peak position of TiO_2 showed a large red shift extending to 520 nm, which indicates that the sensitization of CdS QDs can significantly enhance the photoresponse range of TiO_2. Figure 4b shows the PL spectra of the $CTWT_0$ and $CTWT_3$ sample, with a 260 nm excitation wavelength. The two spectra display identical forms, exhibiting the main character of TiO_2 in PL generation. The main peak at 365 nm can be attributed to the direct recombination of electrons and holes in TiO_2, and the weak peak at 467 nm may be assigned to be the following reasons: the oxygen and impurity defects induced photoluminescence; and the surface states induced photoluminescence at the annealing temperature [33]. Vitally, PL intensity of $CTWT_3$ is lower than that of $CTWT_0$, indicating that TiO_2 can reduce the electron–hole pairs recombination after being deposited on CdS QDs, which contributes to the improvement of the photoelectric performance and photocatalytic activity.

The current–voltage characteristics of the as-prepared samples are shown in Fig. 5a, the photocurrent density increases with increasing applied potential and photocurrent value of the CdS QDs sensitized sample, which is higher than that of bare TiO_2 NWs/NTs arrays. This result indicates that CdS is suited for the sensitization of TiO_2 NWs/NTs arrays. In the case CdS QDs sensitized samples, the current

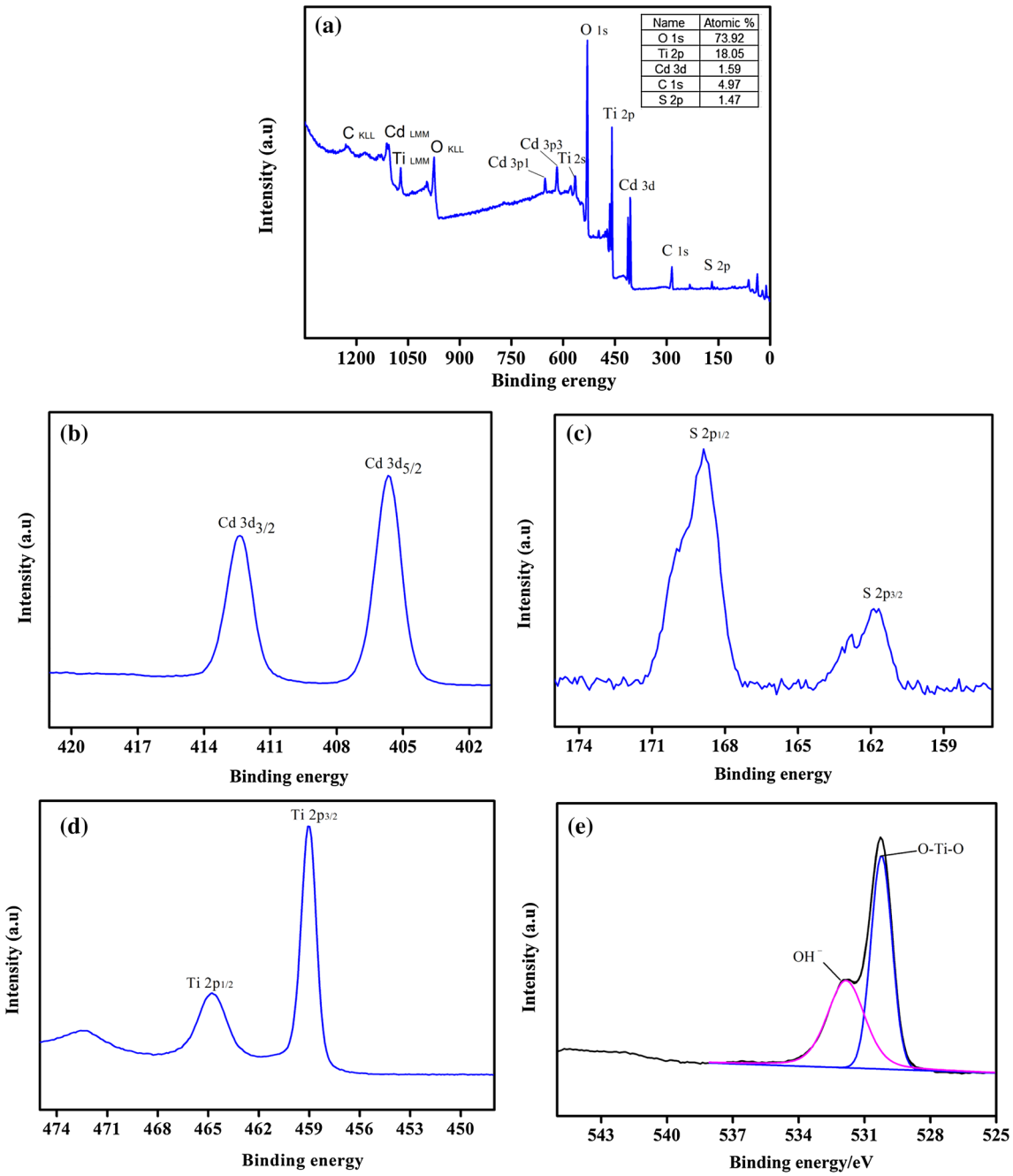

Fig. 3 XPS spectra of sample $CTWT_3$: **a** full spectrum, **b** Cd 3d, **c** S 2p, **d** Ti 2p, **e** O 1s

intensity increased with increasing number of SILAR cycles, in which the maximum value is obtained from the product after 3 cycles. Moreover, the photocurrent onset shifts from −0.111 V (bare) to −0.49 V ($CTWT_3$), which is attribute to a shift in the Fermi level to a more negative potential, resulting a better charge separation and electron accumulation [4].

Figure 5b shows the transient current–time characteristics of the as-prepared samples. A maximum 10% drop down is observed in the whole light process, indicating excellent charge transmission and strong photo stability. At 0.6 V applied potential, the stable photocurrent density of the four samples is 0.375, 0.598, 1.040 and 0.755 mA cm^{-2}, respectively, which shows that those sensitized with CdS QDs are higher than pure TiO_2 NWs/NTS arrays. The highest obtained value is ca. 1.040 mA cm^{-2}, which is ca. 2.8 fold greater than the bare sample (0.375 mA cm^{-2}). Moreover, when the number of SILAR cycles is increased by 5 times, the corresponding

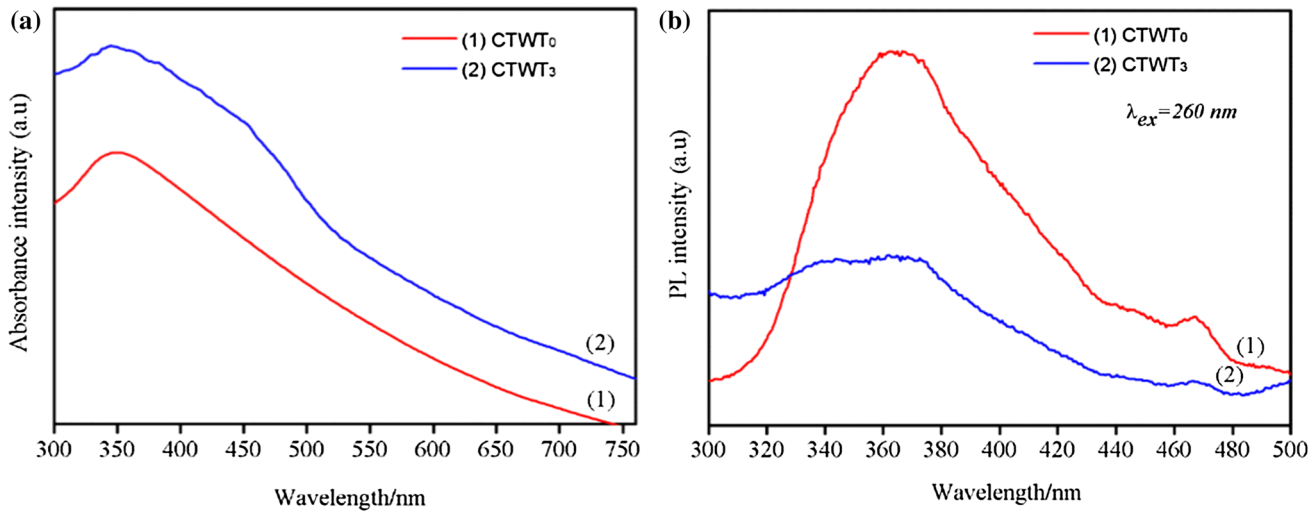

Fig. 4 UV–Vis absorption spectra (**a**) and PL spectra (**b**) of the sample $CTWT_0$ and $CTWT_3$, respectively

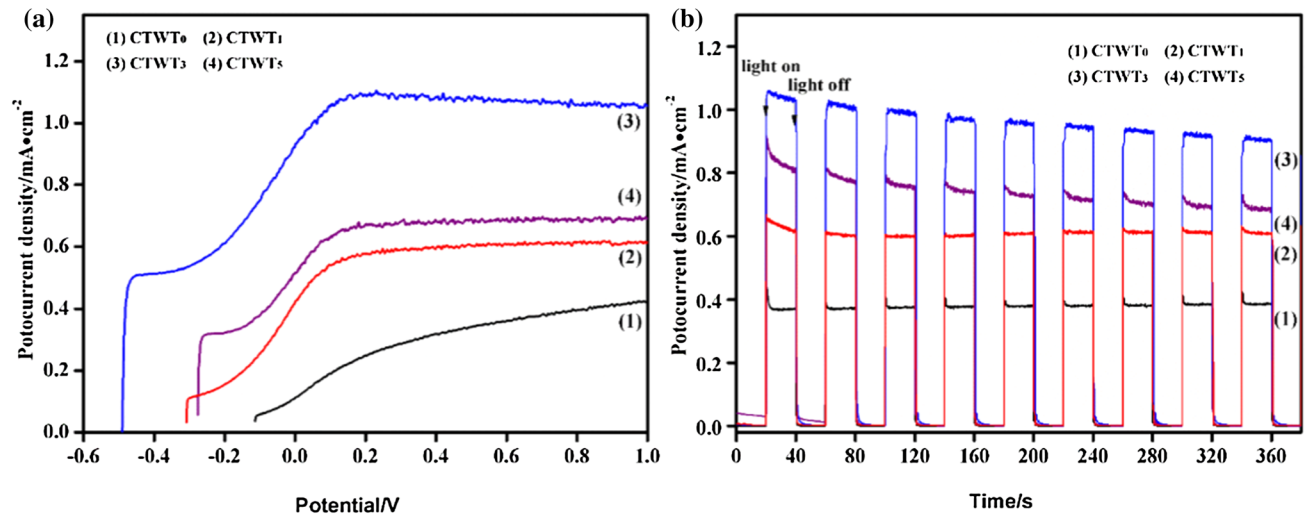

Fig. 5 **a** Current–voltage curves characteristics and **b** transient on–off current–time cycles characteristics of the as-prepared samples

photocurrent density decrease to 0.755 mA cm^{-2}, which is as a result of over surplus dense of the CdS QDs. From the insert imagine of Fig. 1d, QDs were completely wrapped around the TiO_2 NWs/NTS structures and plied arsy-varsy on their surface, which would increase the interface between QDs and hinder charge transfer, hence a decline in photoelectric properties is observed [34].

The photocatalytic activity of these samples was examined under Xe lamp light source at room temperature. The residual concentration of MB solution was detected by UV–Vis spectrophotometer at its characteristic wavelength (λ_{MB} = 663 nm), the ratio of MB concentration C_t/C_0 is calculated by formula (1):

$$C_t / C_0 = A_t / A_0 \quad (1)$$

where C_0 and C_t are the concentration of MB at irradiation time 0 and t, A_0 and A_t are the absorbance intensity at the wavelength of 663 nm at time *0* and *t*, respectively.

As shown in Fig. 6a, 51.8% of MB solution was degraded by the bare TiO_2 NWs/NTs arrays after irradiation for 120 min, which is higher than those previously reported [35], and may attribute to this special composite nanostructure with more reactive sites on their surface. Furthermore, the photodegradation efficiency was increased with the increasing number of SILAR cycles, resulting in the highest degradation rate of 97.8% after 2 h, which is also higher than the same work. Additionally, the absorption spectra of the residual MB solution after degrading by $CTWT_3$ with different time, showing the insert imagine of Fig. 6a. As the intensity of the absorption peak gradually

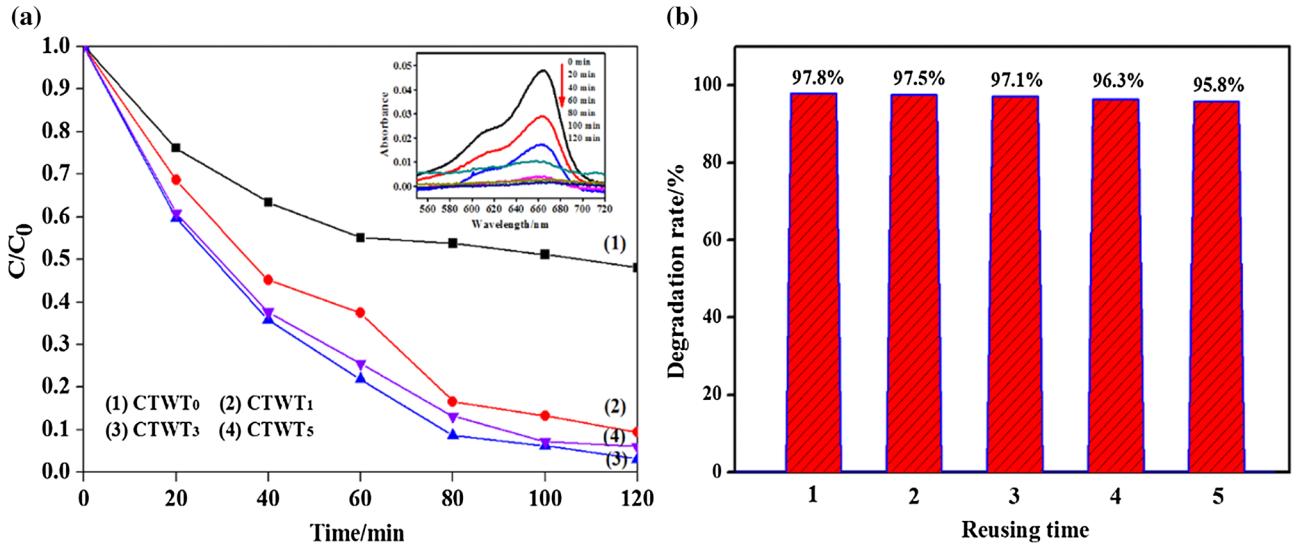

Fig. 6 **a** Photocatalytic activity behavior of the different samples for degrading MB solution (the insert is UV–Vis absorption spectrum of MB solution degrading by the sample $CTWT_3$); **b** stability of the sample $CTWT_3$ for degrading MB solution during a series of 5 identical tests

declined, with a decrease of pollutant concentration, the intensity was almost reduced to zero after 120 min. Meanwhile, the stability of for degrading MB solution was also examined (Fig. 6b), the degradation efficiency was rather stable and the degradation rate was ca. 95.8% after 5 identical tests. This result indicated that the sample displays outstanding properties of stability and reliability for catalyzing the degradation organic pollutants [33].

Summarily, its excellent optoelectronic performance and photocatalytic activity of the prepared sample may be attributed to their excellent structure: CdS QDs possesses a narrow band gap, allowing the absorption spectrum of sensitized TiO_2 to be extended into the visible light region; Nanowires will not only improve the surface area for increasing more reactive sites but also accommodate more QDs, compared with the usual TiO_2 NTs arrays; The QDs deposited on the wall of the tube enable the light to form effective refraction and improve the utilization rate of light; NWs are grown in situ at the mouth of the NTs and closely connect between NWs and NTs, the excited electrons can be rapidly transported along NWs to vertical NTs, reducing the probability of recombination of electron–hole pairs.

4 Conclusion

A new nanostructure of CdS QDs deposited TiO_2 NWs/NTs arrays were successfully fabricated by the anodic oxidation and SILAR cycle process. In this structure, NWs integrated with NTs can enlarge the surface areas for depositing more quantum dots and quickly transport electron to vertical NTs, enhancing the efficiency of photoelectric conversion. Therefore, the as-prepared samples showed an enhancement absorption of visible light, exhibiting an excellent photoelectric and photocatalytic properties. Meanwhile, this structure could be modified by other sensibilizers to further improve their performance and we will also carry out research on this issue. Thus, we believe this strategy of synthetically utilizing the advantages of TiO_2 may provide a prospect for practical application in solar energy and environmental protection.

Acknowledgements This study was funded by the Fundamental Research Funds for the Central Universities Key Project (XDJK2017B062) and the National Science Foundation for Young Scientists of China (Grant No. 51605392).

Compliance with ethical standards

Conflict of interest The authors declare that they have no conflict of interest.

References

1. Li G, Wu L, Li F, Xu PP, Zhang DQ, Li HX (2013) Photoelectrocatalytic degradation of organic pollutants via a CdS quantum dots enhanced TiO_2 nanotube array electrode under visible light irradiation. Nanoscale 5:2118
2. Ge MZ, Li QS, Cao CY, Huang JY, Li SH, Zhang SN, Chen Z, Zhang KQ, Al-Deyab SS, Lai YK (2017) Water splitting: one-dimensional TiO_2 nanotube photocatalysts for solar water splitting. Adv Sci 4:1
3. Bai S, Wang LM, Chen XY, Du JT, Xiong YJ (2015) Chemically exfoliated metallic MoS_2, nanosheets: a promising supporting

co-catalyst for enhancing the photocatalytic performance of TiO_2. Nanocrystals 8:175
4. Xie Y, Ali G, Yoo SH, Cho SO (2010) Sonication-assisted synthesis of CdS quantum-dot-sensitized TiO_2 Nanotube arrays with enhanced photoelectrochemical and photocatalytic activity. ACS Appl Mater Interfaces 2:2910
5. Cao XR, Tian GH, Chen YJ, Zhou J, Zhou W, Tiana CG, Fu HG (2014) Hierarchical composites of TiO_2 nanowire arrays on reduced graphene oxide nanosheets with enhanced photocatalytic hydrogen evolution performance. Mater Chem A 2:4366
6. Zhang JK, Gao Z, Gao HB, Zhao SC, Chen CQ, Chen S, Tong XL, Wang MH, Zheng ZF (2017) Porous TiO_2 nanotubes with spatially separated platinum and CoO_x cocatalysts produced by atomic layer deposition for photocatalytic hydrogen production. Angew Chem 56:816
7. Liu C, Zhang LQ, Liu R, Gao ZF, Yang XP, Tu ZQ, Yang F, Ye ZZ, Cui LS, Xu CM (2016) Hydrothermal synthesis of N-doped TiO_2 nanowires and N-doped graphene heterostructures with enhanced photocatalytic properties. Alloys Compd 656:24
8. Wang WH, Dong JY, Ye XZ, Li Y, Ma YR, Qi LM (2016) Heterostructured TiO_2 nanorod@nanobowl arrays for efficient photoelectrochemical water splitting. Small 12:1469
9. Yang YC, Ji XB, Jing MJ, Hou HS, Zhu YR, Fang LB, Yang XM, Chen QY, Banks CE (2015) Carbon dots supported upon N-doped TiO_2 nanorods applied into sodium and lithium ion batteries. Mater Chem A 3:5648
10. Tian J, Li J, Wei N, Xu XH, Cui HZ, Liu H (2016) Ru nanoparticles decorated TiO_2 nanobelts: a heterostructure towards enhanced photocatalytic activity and gas-phase selective oxidation of benzyl alcohol. Ceram Int 42:1611
11. Carp O, Huisman CL, Reller A (2004) Photoinduced reactivity of titanium dioxide. Progr Solid State Chem 32:177
12. Shankar K, Mor GK, Prakasam HE et al (2007) Highly-ordered TiO_2 nanotube arrays up to 220 µm in length: use in water photoelectrolysis and dye-sensitized solar cells. Nanotechnology 18:5707
13. Ansari SA, Khan MM, Ansari MO, Cho MH (2016) Nitrogen-doped titanium dioxide (N-doped TiO_2) for visible light photocatalysis. Cheminform 47:25
14. Goldstein S, Behar D, Rabani J (2016) Mechanism of visible light photocatalytic oxidation of methanol in aerated aqueous suspensions of carbon-doped TiO_2. Phys Chem C 12:15134
15. Ramandi S, Entezari MH, Ghows N (2017) Sono-synthesis of solar light responsive S–N–C–tri doped TiO_2 photo-catalyst under optimized conditions for degradation and mineralization of diclofenac. Ultrason Sonochem 38:234
16. Zhu K, Neale NR, Miedaner A (2007) Enhanced charge-collection efficiencies and light scattering in dye-sensitized solar cells using oriented TiO_2 nanotubes arrays. Nano Lett 7:69
17. Pastore M, Etienne T, Angelis FD (2016) Structural and electronic properties of dye-sensitized TiO_2 for solar cell applications: from single molecules to self-assembled monolayers. Mater Chem C 4:4346
18. Zhang Z, Li A, Cao SW, Bosman M, Zhou SZ, Xue C (2014) Direct evidence of plasmon enhancement on photocatalytic hydrogen generation over Au/Pt-decorated TiO_2 nanofibers. Nanoscale 6:5217
19. Kumar M, Kumar T, Avasthi DK (2015) Study of thermal annealing induced plasmonic bleaching in Ag: TiO_2 nanocomposite thin films. Scripta Mater 105:46
20. Yoo JE, Altomare M, Mokhtar M, Alshehri A, Al-Thabaiti SA, Mazare A, Schmuki P (2016) Photocatalytic H_2 generation using dewetted Pt-decorated TiO_2 nanotubes: optimized dewetting and oxide crystallization by a multiple annealing process. Phys Chem C 120:15884
21. Dibbell RS, Watson DF (2016) Distance-dependent electron transfer in tethered assemblies of CdS quantum dots and TiO_2 nanoparticles. Phys Chem C 113:3139
22. Lee YL, Huang BM, Chien HT (2016) Highly efficient CdSe-sensitized TiO_2 photoelectrode for quantum-dot-sensitized solar cell applications. Chem Mater 20:6903
23. Li YJ, Ma MJ, Zhu JJ (2016) Dual-signal amplification strategy for ultrasensitive photoelectrochemical immunosensing of α-fetoprotein. Anal Chem 84:10492
24. Lv P, Fu WY, Mu YN, Sun HR, Su S, Chen YL, Yao HZ, Ding D, Liu T, Wang J, Yang HB (2015) Photoelectrochemical property of CdS and PbS cosensitized on the TiO_2, array by novel successive ionic layer adsorption and reaction method. J Alloys Compd 621:30
25. Dong Q, Liao W, Wang B, Liu ZQ (2015) Investigation of interfacial and photoelectrochemical characteristics of thermally treated PbS/TiO_2 photoanodes. RSC Adv 5:33869
26. Hernández-Torres ME, Ojeda-Carrera MT, Sánchez-Cantú M, Gracia-Jiménez JM (2014) CdS/TiO_2 composite films for methylene blue photodecomposition under visible light irradiation and non-photocorrosion of cadmium sulfide. Chem Pap 68:1257
27. Shen QQ, Xue JB, Liu J, Liu XG, Jia HS, Xu BS (2015) Enhancing efficiency of CdS/TiO_2, nanorod arrays solar cell through improving the hydrophilicity of TiO_2, nanorod surface. Sol Energy Mater Sol C 136:206
28. Bai J, Li JH, Liu YB, Zhou BX, Cai WM (2010) A new glass substrate photoelectrocatalytic electrode for efficient visible-light hydrogen production: CdS sensitized TiO_2 nanotube arrays. Appl Catal B Environ 95(3):408–413
29. Liu R, Yang W, Qiang L, Wu J (2011) Fabrication of TiO_2 nanotube arrays by electrochemical anodization in an NH_4F/H_3PO_4 electrolyte. Thin Solid Films 519:6459–6466
30. Li Z, Yu L, Liu Y, Sun S (2014) CdS/CdSe quantum dots co-sensitized TiO_2 nanowire/nanotube solar cells with enhanced efficiency. Electrochim Acta 129:379–388
31. Zou ZJ, Qiu Y, Xie CS, Xu JJ, Luo YS, Wang CL, Yan HL (2015) CdS/TiO_2 nanocomposite film and its enhanced photoelectric responses to dry air and formaldehyde induced by visible light at room temperature. J Alloys Compd 645:17
32. Javid A, Kumar M, Ashraf M, Lee JH, Han JG (2019) Photocatalytic antibacterial study of N-doped TiO_2 thin films synthesized by ICP assisted plasma sputtering method. Physica E 106:187
33. Yina YC, Lia J, Wang YB, Wan J, Du X, Hu XY, Liu EZ, Fan J (2017) Constructing ZnSe and Au co-sensitized TiO_2 nanotube arrays for high-efficiency photoelectrocatalytic activities. Mater Res Bull 88:33
34. Wang HY, Zhu W, Chong BH, Qin K (2014) Improvement of photocatalytic hydrogen generation from CdSe/CdS/TiO_2 nanotube-array coaxial heterogeneous structure. Int J Hydrogen Energy 39(1):90
35. Li H, Chen ZH, Tsang CK, Li Z, Ran X, Lee C, Nie B, Zheng LX, Hung T, Lu J, Pan BC, Li YY (2014) Electrochemical doping of anatase TiO_2 in organic electrolytes for high-performance supercapacitors and photocatalysts. Mater Chem A 2:229